Opposite Effects of Aerosols on Daytime Urban Heat Island Intensity between Summer and Winter

Wenchao Han[1,2], Zhanqing Li[1,2*], Fang Wu[1,2], Yuwei Zhang[3], Jianping Guo[4], Tianning Su[2], Maureen Cribb[2], Tianmeng Chen[4], Jing Wei[1,2], Seoung-Soo Lee[5]

1. State Key Laboratory of Remote Sensing Science, College of Global Change and Earth System Science, Beijing Normal University, Beijing 100875, China
2. Department of Atmospheric and Oceanic Science and Earth System Science Interdisciplinary Center, University of Maryland, College Park, Maryland, 20740, USA
3. Atmospheric Sciences and Global Change Division, Pacific Northwest National Laboratory, Richland, Washington, 99352, USA
4. State Key Laboratory of Severe Weather, Chinese Academy of Meteorological Sciences, Beijing 100081, China
5. San Jose State University Research Foundation, San Jose, California, 95192, USA

Correspondence to: Zhanqing Li (zli@atmos.umd.edu)

Abstract

The urban heat island intensity (UHII) is the temperature difference between urban areas and their rural surroundings. It is commonly attributed to changes in the underlying surface structure caused by urbanization. Air pollution caused by aerosol particles can affect the UHII by changing the surface energy balance and atmospheric thermodynamic structure. By analyzing satellite data and ground-based observations collected from 2001 to 2010 at 35 cities in China and using the WRF-Chem model, we found that aerosols have very different effects on daytime UHII in different seasons: reducing the UHII in summer, but increasing the UHII in winter. The seasonal contrast in the spatial distribution of aerosols between the urban centers and the suburbs lead to a spatial discrepancy in aerosol radiative effect (SD-ARE). Additionally, different stability of the planetary boundary layer induced by aerosol is closely associated with a dynamic effect (DE) on the UHII. SD-ARE reduces the amount of radiation reaching

30   the ground and changes the vertical temperature gradient, whereas DE increases the stability of the planetary boundary layer and weakens heat release and exchange between the surface and the PBL. Both effects exist under polluted conditions, but their relative roles are opposite between the two seasons. It is the joint effects of the SD-ARE and the DE that drive the UHII to behave differently in different seasons, which is confirmed by model simulations. In summer, the UHII is mainly affected by the SD-ARE, and

35   the DE is weak, and the opposite is the case in winter. This finding sheds a new light on the impact of the interaction between urbanization-induced surface changes and air pollution on urban climate.

1.   Introduction

The global population has been increasingly concentrated in cities (Heilig 2012). Urbanization in China

40   has dramatically increased from 26% in 1990 to 60% in 2018, resulting in a marked change of landscape. It has a significant impact on the urban and rural climate and will continue to make an impact as cities continue to develop (Han et al. 2014).

Urbanization leads to a dramatic change in the underlying surface structure, properties, and spatial distribution of a city, such as a reduction in green areas and a corresponding increase in impervious areas.

45   These changes increase the temperature difference between urban and rural areas, which is known as the urban heat island (UHI) intensity (UHII) (e.g., Kalnay and Cai 2003, Zhao et al. 2014, Zhao et al. 2016, Zhou et al. 2016, Yang et al. 2017). The UHI also affects the structure and movement of cloud systems (Changnon and Westcott 2002, Kug and Ahn 2013, Pinto et al. 2013). The diurnally and seasonally varying UHI is affected by many factors, such as weather and climatic regimes, urban impervious surfaces,

50   anthropogenic heat, air pollution, and urban 3D structure (Oke 1982, Morris and Simmonds 2000, Kim and Baik 2002, Gedzelman et al. 2003, Ryu and Baik 2012, Ding et al. 2016, Yang Y et al. 2019). It is well established that cities are the largest sources of anthropogenic heat emissions as by-products from industrial and human activities. Human activities can also generate large amounts of aerosols that can reduce air quality, change the physical and chemical properties of the atmosphere, and endanger human

55   health (Sanap and Pandithurai 2015, Cohen et al. 2017, Wei et al. 2019a, b). With increasing urbanization in the future, cities are likely to influence local and regional weather and climate to greater degrees.

Aerosols can also alter the radiation balance of the climate system. Their thermodynamic effect reduces the amount of radiation reaching the ground, and their microphysical effect can influence cloud properties and precipitation regimes through their impacts on cloud microphysical and dynamic processes
60 (Rosenfeld et al. 2008, Li et al. 2011, Fan et al. 2013, Li et al. 2016, Guo et al. 2018, Liu et al. 2019). The effect of urbanization on clouds and precipitation has been the focus of many studies (Changnon et al. 1977, Ackerman et al. 1978, Changnon et al. 1991, Shepherd et al. 2002, Shepherd and Burian 2003). Aerosols can increase cloudiness and cloud thickness and thus change the stability of the planetary boundary layer. In humid regions, aerosols may reduce the frequency of light rain but increase heavy
65 rainfall, while in dry areas, aerosols aggravate droughts. Aerosols can also intensify convection by delaying the occurrence of convection and enhancing gust fronts (Khain et al. 2005, Carrió et al. 2010, Carrió and Cotton 2011, Wang et al. 2011, Han et al. 2012, Lee and Feingold 2013, Li et al. 2017, Guo et al., 2016a).

UHI, surface roughness and higher aerosol concentrations have been proposed to explain observed urban
70 clouds and precipitation anomalies. Increased urban surface roughness likely does not play a major role in urban-induced precipitation. Rather, the UHI and higher aerosol concentrations may play more important roles (Han et al. 2014). The UHI can alter the water vapor flux (accelerate evaporation), reduce horizontal wind speeds and enhance vertical turbulence, reduce the temperature difference between daytime and nighttime, increase the absorption rate of solar radiation by land, and change underlying
75 surface characteristics (e.g., sensible heat dissipation, convection efficiency, evaporation and cooling, sunlight reflection, and anthropogenic heat transfer) (Jauregui and Romales 1996, Taha 1997, Bornstein and Lin 2000, Givati and Rosenfeld 2004, Grimmond 2007, Carrió et al. 2010, Zhao et al. 2014, Kaspersen et al. 2015, Yang B et al. 2019).

The UHI and aerosols may interact over cities. Aerosols generally reflect and absorb solar radiation and
80 reduce the amount of shortwave radiation reaching the ground, i.e., the cooling effect of aerosols on ground temperature. Some numerical modelling studies have demonstrated that landscape change reduces near-surface concentrations of $PM_{2.5}$ and that the UHI effect can influence the dispersion of air pollutants (Liu et al. 2009, Liao et al. 2015, Tao et al. 2015, Zhong et al. 2017, 2018). Moreover, aerosols can enhance the UHI at night (by 0.7±0.3 K) for semi-arid cities, and the UHI alters the aerosol concentration

85 (Cao et al. 2016, Fallmann et al. 2016, Lai 2016). Heavy pollution can reduce UHII in China, especially during the day (Wu et al. 2017, Yang et al. 2020).

Weather Research and Forecasting/Chemistry (WRF-Chem) model are used extensively in the simulation and prediction of air quality, the aerosol radiation effect and aerosol-cloud interactions, and the change of meteorological fields and regional climate (Grell et al. 2005, Chapman et al. 2009). Coupled with the

90 urban canopy model, WRF can account for the influences of aerosols and land surface changes on the radiative processes if such parameters are fed to the model as aerosol loading and single scattering albedo, surface albedo and thermal emissivity, roughness, etc (Miao et al. 2009, Chen et al. 2011). Many previous pertinent studies are done to date just focused on the annual effects without investigating any seasonal differences and the underlying mechanism. This study aims to fill this gap by analyzing the annual and

95 seasonal effects of aerosols on UHII and proposing mechanisms that may explain the seasonal differences.

2. Methods

2.1 Study areas and data

Thirty-five big cities evenly distributed across China were selected in our study. Table S1 lists these cities

100 of different sizes. They represent the major and well-developed metropolitan regions in China. The population and urban areas of these cities have increased faster and/or more dramatic than those of other cities from 2001 to 2015.

Data used in this study include Land Satellite Thematic Mapper/ Enhanced Thematic Mapper (Landsat TM/ETM+) and Moderate Resolution Imaging Spectroradiometer (MODIS) products [including land

105 surface temperature (LST) and aerosol optical depth (AOD)], ground-based data from meteorological stations, particulate matter ($PM_{2.5}$) concentrations, and sounding data.

Landsat data are used to identify and outline urban areas and urban contour. The spatial resolution is 30 m. Summertime (June, July, and August) images from 2000 and 2015 were examined to ensure the accuracy and consistency of results.

110 The MODIS LST product (MYD11A2) at a 1-km spatial resolution was used to calculate urban and rural UHIIs. Since this study is mainly focused on the daytime UHI effect, only data (eight-day clear-sky LST observations with 1 km spatial resolution) at 13:30 BJT for the period 2001–2015 were used. The

MYD11A2 product uses the MODIS cloud mask product (MYD35) to filter out cloudy conditions. A generalized split-window algorithm is applied using MODIS data in two longwave bands in the

115   atmospheric window to correct for atmospheric water vapor, haze effects, and the sensitivity to errors in the surface emissivity. To obtain the LST from brightness temperatures, changes in surface emissivity have been accounted for (Wan and Dozier 1996, Snyder et al. 1998, Wang and Liang 2009, Yu et al. 2011, Cao et al. 2016).

The MODIS Multi-Angle Implementation of Atmospheric Correction (MAIAC) AOD product is used

120   that has a 1-km spatial resolution with daily global coverage. It was retrieved by virtue of a time series analysis and a combination of pixel- and image-based processing to improve the accuracies of cloud detection, aerosol retrievals, and atmospheric correction (Lyapustin et al. 2011a, 2011b, 2012).

A large volume of meteorological data are analyzed including visibility, surface wind speed, temperature, precipitation, and other parameters every three hours, together with hourly $PM_{2.5}$ data in urban and

125   surrounding rural areas. To be consistent with the satellite imaging time (13:30 BJT), the meteorological data and $PM_{2.5}$ data observed at 13:00 and 14:00 BJT are selected. Due to the lack of long-term records of aerosol concentration, visibility is frequently used as a proxy for aerosol loading (Wang et al. 2009, Wu et al. 2012, Yang et al. 2013).

The L-band sounding data are employed that were acquired at the five radiosonde stations in Beijing,

130   Chengdu, Nanjing, Shenyang, and Xi'an operated by the China Meteorological Administration since 2006. They contain the high-resolution profiles of temperature, pressure, relative humidity, and wind speed and direction at 08:00 Beijing time (BJT, UTC+8) and 20:00 BJT (Zhang et al., 2018; Lou et al., 2019). The data quality of radiosonde measurements has been well validated and is good enough to study the UHI effect (Guo et al., 2016b).

135

2.2 Extracting urban impervious surfaces and urban contours

Indices commonly used to extract built-up areas include the Difference Built-up Index (DBI), the Index-based Built-Up Index (IBI), and the Normalized Difference Built-up Index (NDBI). Another index, the Soil-adjusted Vegetation Index (SAVI), is a modification of the normalized difference vegetation index

140   that corrects for the influence of *soil* brightness when the vegetative cover is low (Huete 1988, Qi et al.

1994, Rondeaux et al. 1996). After some tests, the difference $NDBI - SAVI$ were used to extract urban

impervious surfaces because of its ability to differentiate urban impervious surfaces from other land-use

types:

$$NDBI = \frac{\rho_5 - \rho_4}{\rho_5 + \rho_4}, \qquad\qquad (1)$$

145    $$SAVI = \frac{\rho_4 - \rho_3}{\rho_4 + \rho_2 + L}(1 + L), \qquad\qquad (2)$$

where L is the soil adjustment factor whose value is 0.5, and ρ_n is the Landsat reflectance of band n. We

then used different thresholds to extract urban impervious surfaces after calculating $NDBI - SAVI$.

Results are verified by the Google Earth and a land-use map with a 1:100,000 scale from the Resource

and Environment Science Data Center of the Chinese Academy of Sciences.

150

2.3 Research windows

Many previous studies have extracted urban areas from nighttime stable-light data. However, the spatial

resolution of such data is low, so the extraction accuracy would be significantly affected in urban areas

with uneven zoning and in regions with irregular urban development as in most municipalities in China.

155   The TM/ETM+ data are used to accurately extract the physical boundaries of urban areas. The difference

in the underlying surfaces of urban and rural areas forms the basis of the urban physical boundary

extraction. Urban surfaces are generally covered by impervious materials, and rural surfaces are mainly

covered by natural surfaces. The influence of the UHI is not only felt within the physical boundaries of

urban areas but also beyond it. In terms of area, this influence can extend to 2–4 times the extent of an

160   urban area. In terms of distance, the influence of the UHI can be felt as far as 3–6 km away from an urban

physical boundary (Zhou et al. 2015).

For each city, nine research windows (6 km x 6 km each) were selected. The windows include one urban

window, four suburban windows, and four rural windows. For the study period considered (2001–2015),

the urban window represents an area that remained urban and developed during this time. The suburban

165   windows represent areas that were vegetated before the study period. As cities expand, these areas were

gradually replaced by urban impervious surfaces from 2001 to 2015. The rural windows represent areas

Atmospheric
Chemistry
and Physics
Discussions

Open Access

EGU

that remained vegetated during the study period. These windows were 10 km away from the urban

physical boundary to ensure that these windows were not or weakly affected by the UHI. The elevations

of the areas covered by each window are within 100 m of each other for a given city based on DEM

170 (Digital Elevation Model) data. Water bodies are excluded. Figure S1 shows the spatial distribution of

the nine research windows for a given city. The UHII is the temperature difference between the average

temperature of the urban core window and the average temperature of rural windows.

2.4 Aerosol parameters (AOD, PM2.5)

175 Validation using Aerosol Robotic Network AOD retrievals shows that the MAIAC and MODIS aerosol

retrieval algorithms have similar accuracies over dark and vegetated surfaces and that the MAIAC

algorithm generally improves the accuracies of AOD retrievals over bright surfaces such as deserts and

urban surfaces (Lyapustin, et al. 2011a, 2011b, 2012, Wei et al., 2019c, Zhang et al. 2019). Sounding data

and $PM_{2.5}$ measurements were available from 2013 to 2015. MAIAC AOD retrievals for each area were

180 averaged to obtain the spatial distribution of AOD over each city, then the difference of AOD between

urban and rural areas was calculated.

2.5 WRF-Chem model simulation

The model used in this study is WRF-Chem 3.9.1 coupled with a single-layer urban canopy model. As

185 shown in Figure S6, the domain with a horizontal grid resolution of 3 km and 50 vertical levels from the

surface to 50 hPa is used. To better characterize the planetary boundary layer, 16 layers are set below

1km, of which the first layer is about 47m in Beijing. Meteorological fields are provided by the National

Centers for Environmental Prediction Final Analysis data (NCEP-FNL) with 6-h temporal frequency and

$1°\times1°$ spatial resolution. The chemical lateral boundary and initial conditions were provided by GEOS-

190 CHEM model. The land cover is derived from the IGBP-Modified MODIS 20-category Land Use

Categories dataset. Monthly $0.25°\times0.25°$ anthropogenic emissions of aerosols and precursors are obtained

from the Multi-resolution Emission Inventory for China (MEIC, 2012) (http://www.meicmodel.org),

which provide monthly mean emission data of SO_2, NO_x, CO, NMVOC, NH_3, BC, OC, PM2.5, PM10, and

CO_2. The biogenic emission data is provided by the Model of Emissions of Gases and Aerosols from

195 Nature (MEGAN) (Guenther et al., 2006. Sakulyanontvittaya et al., 2008). The Fire Inventory from

NCAR (FINN) model provides the biomass burning emission data (Wiedinmyer et al., 2011). Carbon-

Bond Mechanism version Z (CBMZ) chemical mechanism and Model for Simulating Aerosol Interactions

and Chemistry (MOSAIC) are used in this simulation (Zaveri and Peters 1999, Zaveri et al. 2008). Other

details of schemes used in simulations are shown in Table S3. The simulations are initiated at 1200 UTC

200 30 June 2015 for summer and 1200 UTC 01 January 2015 for winter. The meteorological fields are

reinitialized every 48 hours. We conducted four sets of model experiments (Table S2) to investigate the

aerosol radiative impact for both summer and winter (a) A1Summer with aerosol radiative effect turned

on, (b) A0Summer with aerosol radiative effect turned off, (c) A1Winter with aerosol radiative effect

turned on, and (d) A0Winter with aerosol radiative effect turned off. To be consistent with the observation

205 analysis, we select clear-day simulations as the analysis time period by excluding the first 3-day

simulation for chemistry spin-up (Table S2).

3. The Urban Heat Island (UHI) effect

We used the difference NDBI − SAVI to extract urban impervious surfaces, and then determined urban

210 contours based on the identification of impervious surfaces. Figure 1 shows the urban contours of all

cities.
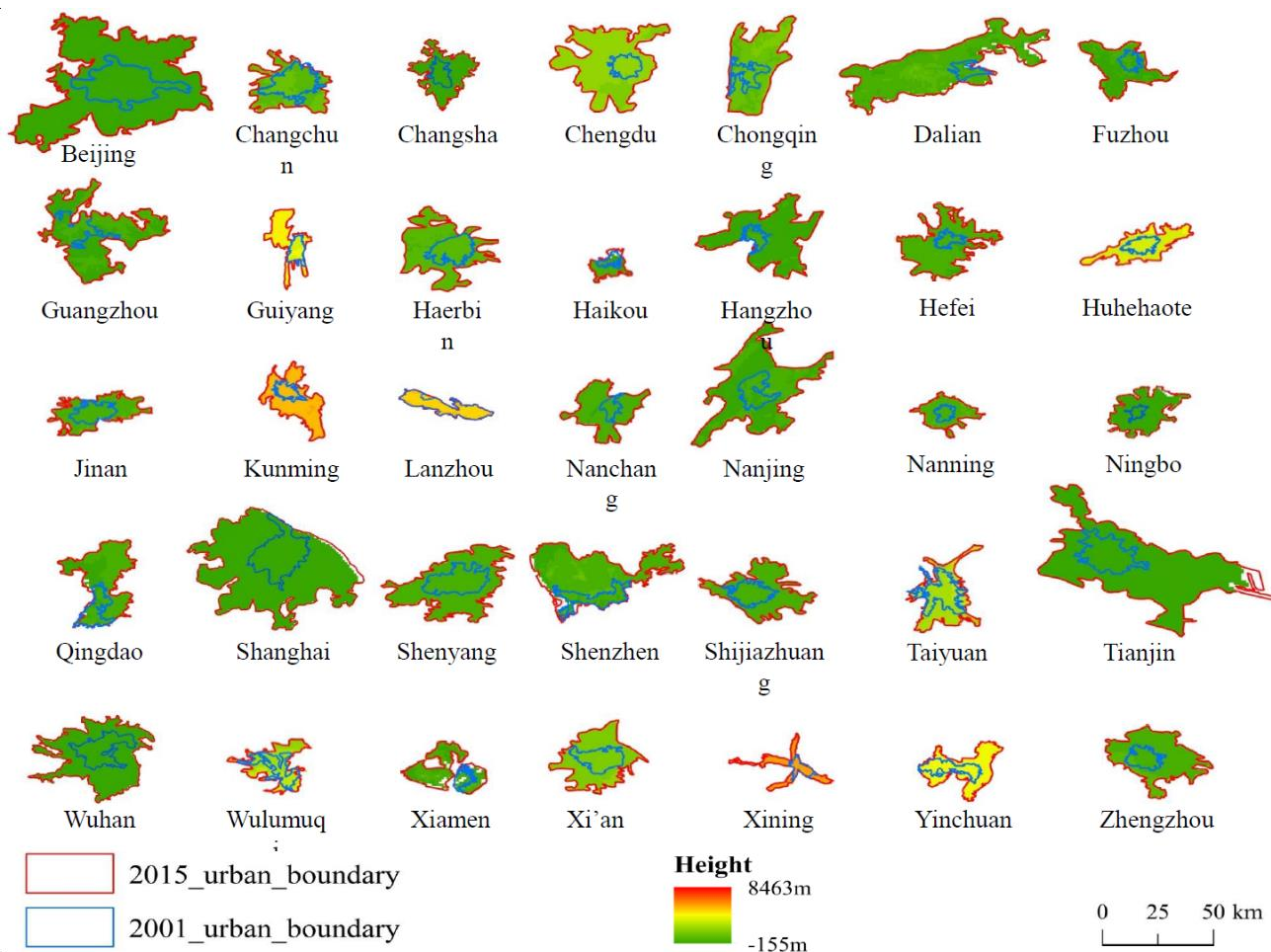
Figure 1. Main urban contours of the 35 cities. Blue contours outline urban boundaries in 2001 and red contours urban boundaries in 2015. The surface height (in meters above sea level) is indicated by color shading.

Figure S2 shows UHII and visibility trends. For most cities, no matter before or after 2008, there are similar trends between UHII and visibility; and there is an obvious difference between trend before 2008 and trend after 2008 of both UHII and visibility. Figure 2 shows the relationships between UHII and visibility based on their respective trends shown in Figure S2. UHII and visibility are positively correlated grossly. Higher visibility means a lower aerosol concentration, leading to a higher UHII, and vice-versa. On the other hand, the two may also change in opposite directions if the expansion of a city is more associated with the heavy industry of strong emissions. In such a case, the expansion can produce both

9

Atmospheric
Chemistry
and Physics
Discussions
Open Access
EGU

more aerosol particles, especially secondary aerosols converted from precursor gases, and stronger UHI,

225 but they have no causal relation. This is likely a reason for the diverse relationships between the trends of the two variables. Of course, the complication originates from highly different pathways of city expansions among these cities. The overall positive relationships revealed in Figure 2 may thus serve as a testimony to the dominance of their causal relationship, implying that aerosol loading does influence the UHII to a varying degree.
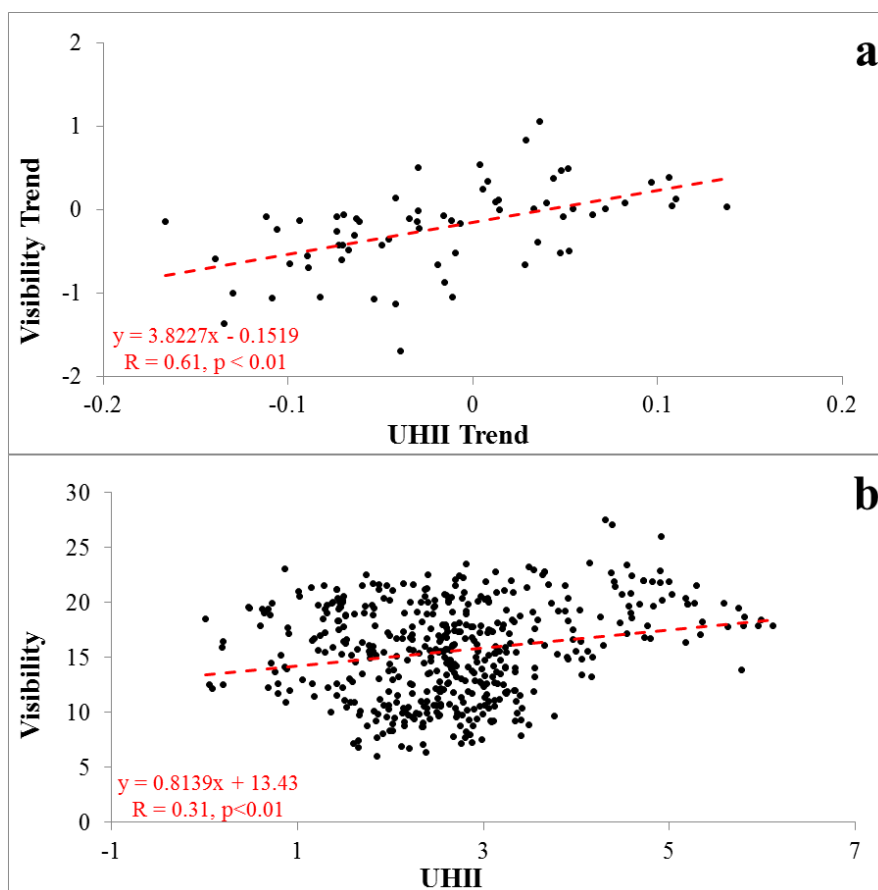
Figure 2. (a) Visibility trend (unit: km yr^{-1}) shown as a function of the UHII trend (K yr^{-1}), and (b) visibility (unit: km) shown as a function of UHII (unit: K). The blue line is the linear best-fit line through the points. The least-squares regression equation is given in each panel. The coefficient correlation (R) and p-value are also given.

235

In order to better investigate the effect of aerosols on the UHII, we calculated the UHII under severe air pollution conditions (i.e., visibility less than 8 km) and compared it with the average UHII:

$$MUHII = \frac{\sum_{i=1}^{n=15} UHII_{m\sim i} - UHII_{p\sim i}}{n}, \qquad (3)$$

where $MUHII$ is the difference between the UHII under severe air pollution conditions and the average

240   UHII, n is number of years from 2001 to 2015, i represents a specific year during 2001–2015, $UHII_{m\sim i}$

is the average UHII in year i, and $UHII_{p\sim i}$ is the UHII under severe air pollution conditions in a year i.

Figure S3 shows the $MUH11$ at each city under polluted conditions and for all days. On an annual scale,

the UHII under severe air pollution conditions is lower than the average UHII, which suggests that a high

aerosol loading will reduce the UHII. In summer (Figure 3a), the UHI at 29 of the 35 cities is weaker

245   under polluted conditions. In winter (Figure 3b), however, it is just opposite, with the majority (27 out of

35) cities having stronger UHI under polluted conditions, suggesting that aerosols enhance the UHII in

winter.
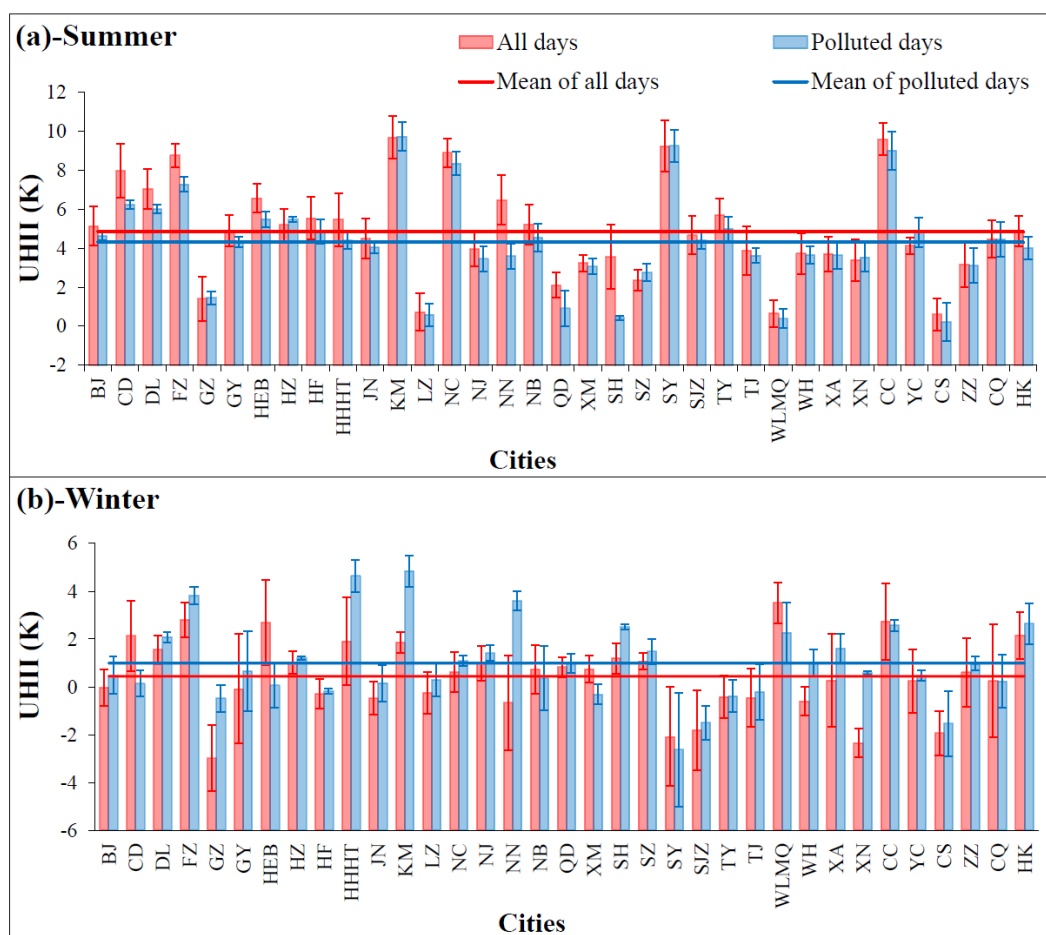
Figure 3. The mean UHII (unit: K) at the 35 cities in (a) summer and (b) winter. Red and blue bars
250 represent UHII calculated using data from all days and from polluted days only, respectively. The overall
mean UHII calculated using data from aS4ll days and from polluted days only are shown as red and blue
solid lines, respectively.

4. Causes for the opposite impacts of aerosol on the UHI in summer and winter

255 **4.1 Mechanisms of aerosol impact on the UHI**

Aerosols alter radiation budget by scattering and absorbing solar radiation (Chylek and Coakley 1974,
Chylek and Wong 1995, Li 1998). The aerosol radiative effect tends to cool down surface, warm up the
atmosphere, stabilize the PBL, suppress the dispersion of pollutants in the PBL to incur a positive
feedback (Li et al. 2017). As illustrated in Figure 4, the UHII may be influenced by both the Spattial
260 Discrepancy of Aerosol Radiative Effect (SD-ARE) and the suppressed vertical exchange of surface heat
fluxes which may be denoted as the Dynamic Effect (DE) for it is related to turbulent dynamics.
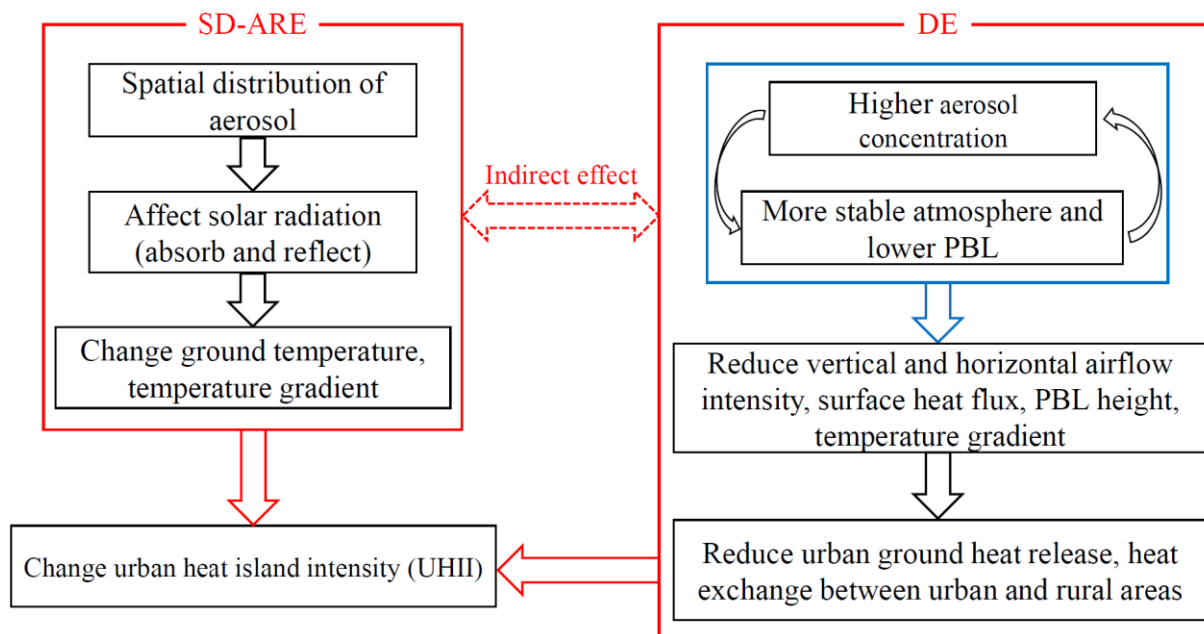
Figure 4. Diagram of the mechanisms behind aerosol effects on the UHII. The blue frame contains the
processes and interactions between aerosols and the PBL. Red frames contain the processes of the Spatial
265 Discrepancy of Aerosol Radiative Effect (SD-ARE) and the Dynamic Effect (DE), respectively. The solid
arrows denote the direct effect, while the dashed arrow indicates the indirect effect.

The Spatial Discrepancy of Aerosol Radiative Effect (SD-ARE): The varying amount of solar radiation reaching the ground between urban and rural areas influences the rise of the LST and thus changes UHII,

270   as a result of different aerosol loading and properties between urban and rural areas. This process has a negative effect on UHII.

The Dynamic Effect (DE): On the other hand, aerosol-induced temperature inversion (especially in winter) within the PBL (Zhang et al. 2014, Li et al. 2015, Li et al. 2017) renders very stable PBL to inhibit vertical and horizontal airflows and surface heat fluxes (latent/sensible heat) between urban areas and rural areas

275   (Petäjä et al. 2016). Urban surfaces can store more heat which affects the UHII. This process has a positive effect on UHII.

Compared with rural areas, urban impervious surfaces have low thermal capacity and their temperatures are thus more sensitive to heat changes. Note that the DE and SNA-RE are not independent and that there is an indirect effect between them due to potential urban-rural circulation.

280

4.2 Analyses of Influential factors

Urban-rural differences in air quality: The urban-rural differences in air quality were analyzed by calculating the spatial differences of $PM_{2.5}$ and AOD under cloudless conditions between urban and rural areas. Their spatial differences are then analyzed between summer and winter:

285   The measurements of urban $PM_{2.5}$ concentrations were divided into four categories: 0–50, 50–100, 100–150, and > 150 μg m^{-3} based on urban pollution. Figure 5 shows the mean urban-rural differences in each $PM_{2.5}$ concentration bin of all cities. On average, the spatial difference in summer is larger than in winter across all $PM_{2.5}$ concentration bins. Figure 6 shows the variation trends of mean AOD as a function of distance from the urban geometrical center of each city in winter and summer. As the distance from the

290   urban geometrical center increases, summertime AODs decrease more rapidly than wintertime AODs. Both Figures 5 and 6 indicate that the spatial difference of air pollution between urban and rural areas in summer is larger than that in winter. Moreover, in summer, urban pollution is often more serious than rural pollution. In winter, both urban and rural pollution is serious, and rural may be more serious than urban.

Atmospheric
Chemistry
and Physics
Discussions
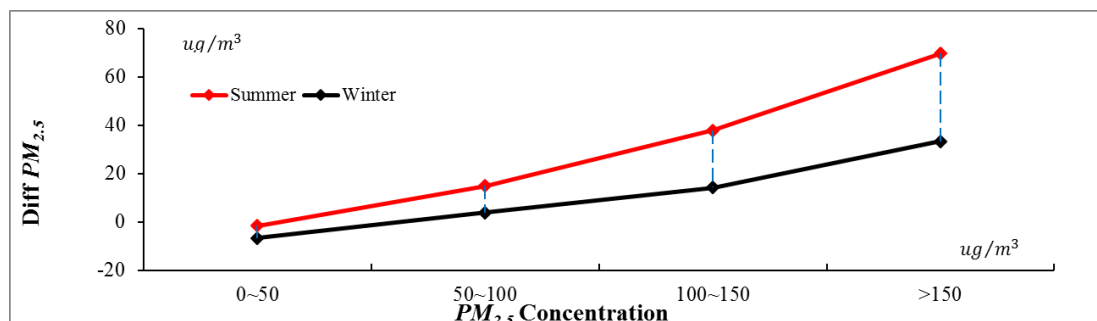
Figure 5. Summertime (red curves) and wintertime (black curves) urban-rural $PM_{2.5}$ (unit: μg m^{-3}) differences of all cities across four $PM_{2.5}$ concentration bins: 0–50, 50–100, 100–150, and > 150 μg m^{-3}.
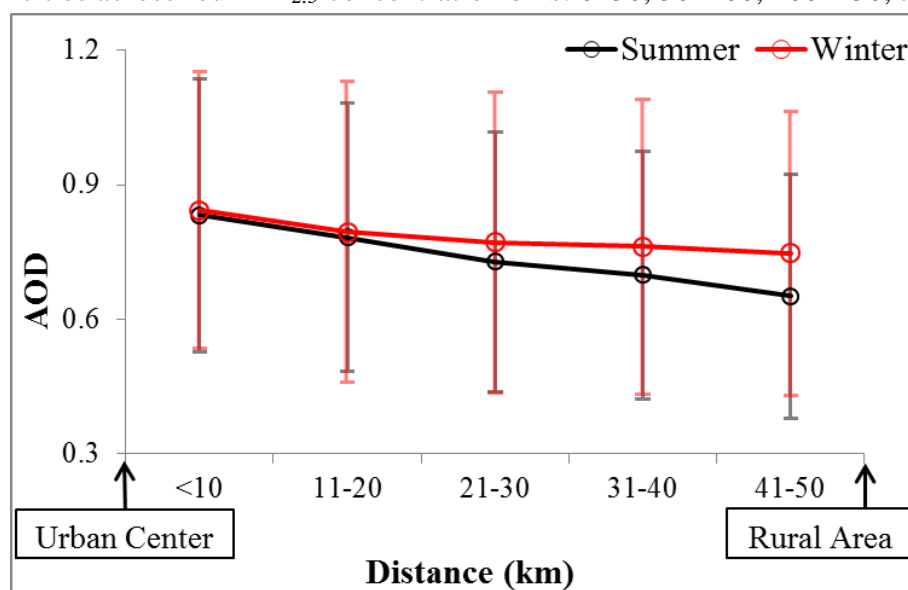
Figure 6. Mean AOD as a function of distance from the urban geometrical center of all cities in winter (red curves with open circles) and summer (black curves with crosses). The distance ranges are < 10 km, 11–20 km, 21–31 km, 31–40 km, and 41–50 km from the urban geometrical center.

Air stability inside the PBL: Wind affects the heat exchange between urban and rural areas, regardless of wind direction, high wind speed favors urban-rural heat exchange and reduces the UHII, while low wind speed decrease urban-rural heat exchange and enhance UHII. The means of wind speed are computed in urban and rural areas in summer and winter, under polluted and clean conditions (Figure 7). As is expected, the mean wind speed under polluted conditions is lower than that under clean conditions, especially in

14

winter when the difference is 1.1 ms^{-1} v.s. 0.6 ms^{-1} in summer. This result indicates that the urban-rural exchange in summer is stronger than that in winter.
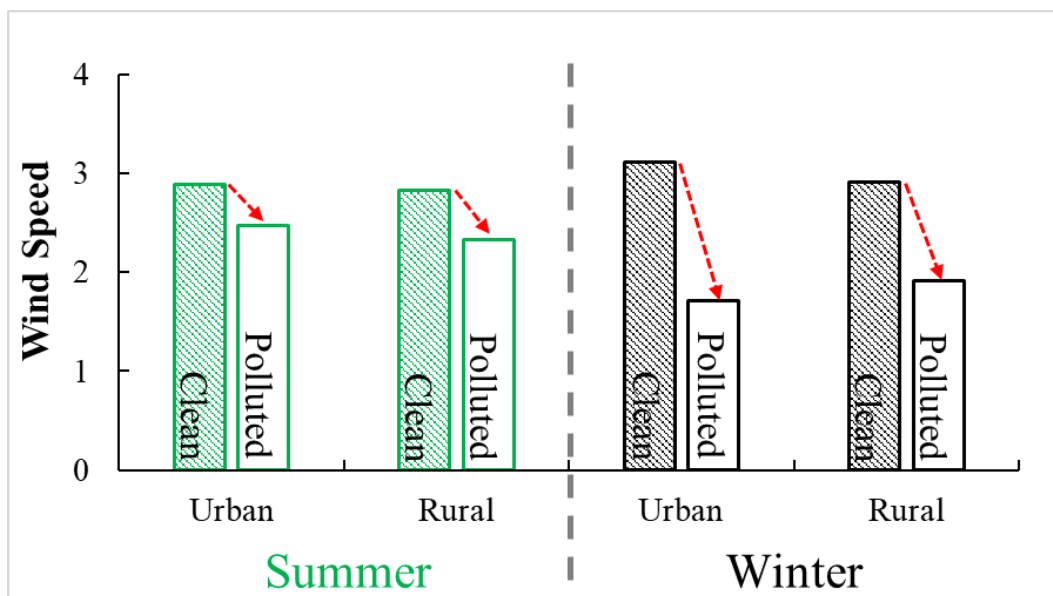
310

Figure 7. Comparison of average wind speed (unit: m s^{-1}) of 35 cities between urban and rural areas under heavy air pollution (white bars) and clean conditions (dark bars) in summer and winter, respectively.

Vertical temperature gradients affect the stability of the atmosphere, surface heat fluxes (especially
315 sensible heat) and vertical turbulence. Figure 8 shows the vertical temperature profiles at five cities in different seasons under polluted and clean conditions. Note that there are much fewer sounding stations than general surface meteorological stations in China. The vertical temperature gradient is weaker under polluted conditions than under clean conditions, so the vertical mixing is weaker. This phenomenon is also more pronounced in winter than in summer. The temperature gradient within the planetary boundary
320 layer (PBL) under polluted conditions generally decreases more drastically than under clean conditions, except at Chengdu that is located in the Sichuan Basin. The temperature lapse rate is smallest under polluted conditions in winter (Figure 9). These results suggest that compared with clean conditions, vertical airflow and surface heat release under polluted conditions are lessened more significantly in winter than in summer.

Atmospheric
Chemistry
and Physics
Discussions
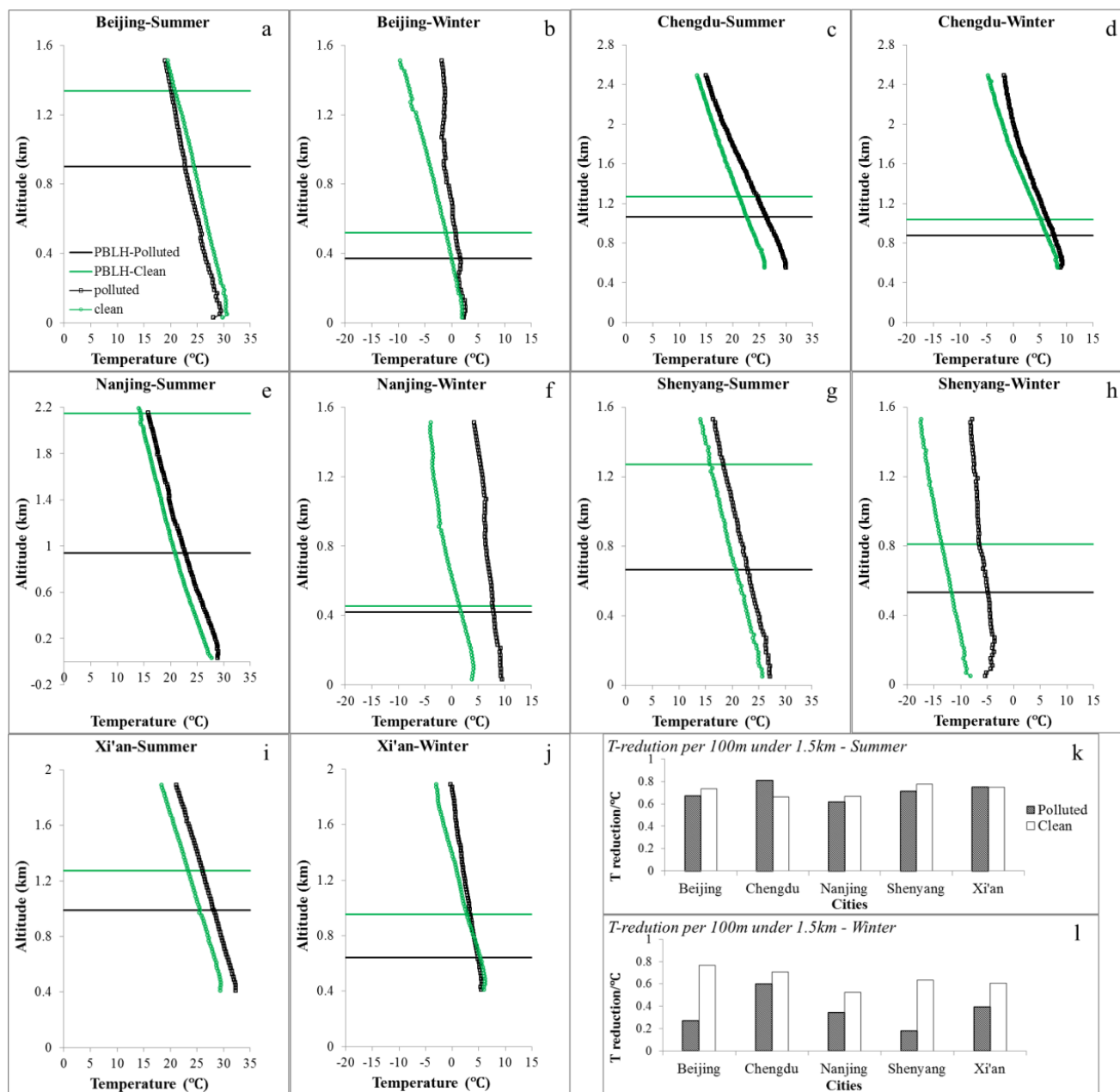
Figure 8. Mean vertical temperature profiles (vertical curves, unit ℃) at five cities in different seasons and under polluted (black) and clean (green) conditions. The mean PBL heights (PBLH) under polluted and clean conditions are also shown (black and green horizontal lines, respectively). Panels (a), (c), (e), (g), and (i) show summertime results, and panels (d), (f), (h) and (j) show wintertime results. Panels (k) and (l) show temperature reductions below 1.5 km [unit: ℃ (100 m)$^{-1}$] under polluted (dark bars) and clean (white bars) conditions in summer and winter, respectively.
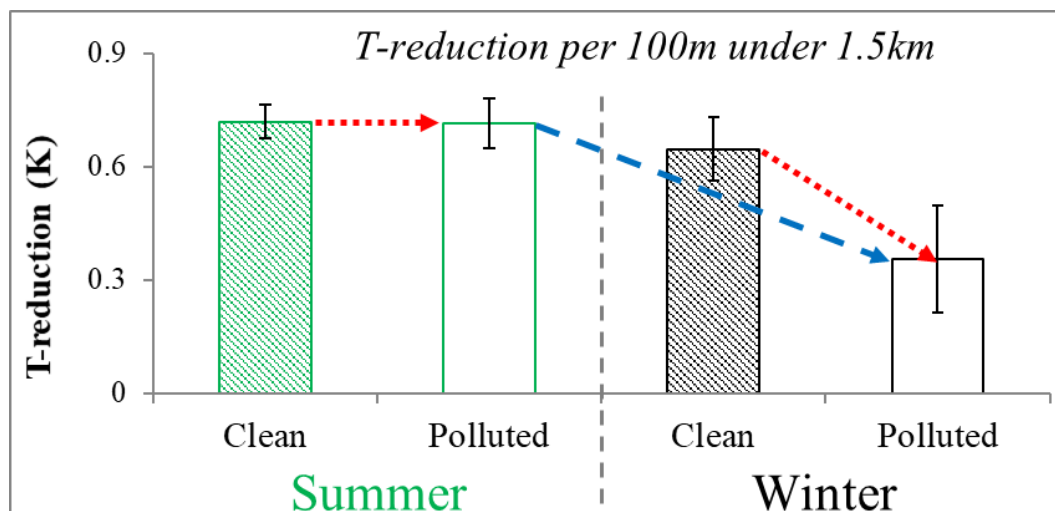
Figure 9. The average temperature reductions of sounding observations of five cities below 1.5 km [unit: K $(100\ m)^{-1}$] under polluted (dark bars) and clean (white bars) conditions in summer and winter, respectively.

Seasonal differences in air stability in the urban and rural areas may be summarized as follows. Under polluted conditions, both horizontal and vertical exchanges decrease inside the PBL, thus weakens the heat exchange and pollution dispersion. However, this effect is much stronger in winter than in summer. In winter, airflow significantly weakens with the increasing pollution, the PBL becomes very stable, and heat exchanges significantly decrease inside the PBL.

UHII response to variation of visibility: Figure S5 shows the relationship between UHII and visibility difference. For most cities, higher visibility difference causes smaller UHII in summer, while UHII barely changes as visibility difference change in winter. This result indicates that UHII is more sensitive for visibility difference in summer than winter, namely, the SD-ARE has an obvious effect in summer, but it is very weak in winter.

The above analyses indicate that the two mechanisms behave differently roles in summer and winter. In summer, the SD-ARE plays a more important role than the DE to change the UHII, while the importance of two mechanisms is opposite in winter.

4.3 Testing the mechanisms by modeling

Atmospheric
Chemistry
and Physics
Discussions

We evaluate the simulated aerosol and meteorological properties with surface $PM_{2.5}$ observation and sounding data (Figure S6, S7 and 10). Figure S6 shows that the simulated $PM_{2.5}$ near-surface get high concentrations at the regions south of Beijing and east to Beijing, in general agreement with the

355 observation. The temporal variations of simulated $PM_{2.5}$ concentrations have consistent trends as observation for most stations (Figure S7). The vertical profiles of temperature, RH and wind speeds also agree with the sound in observation. Therefore, the simulation results are sound in general.
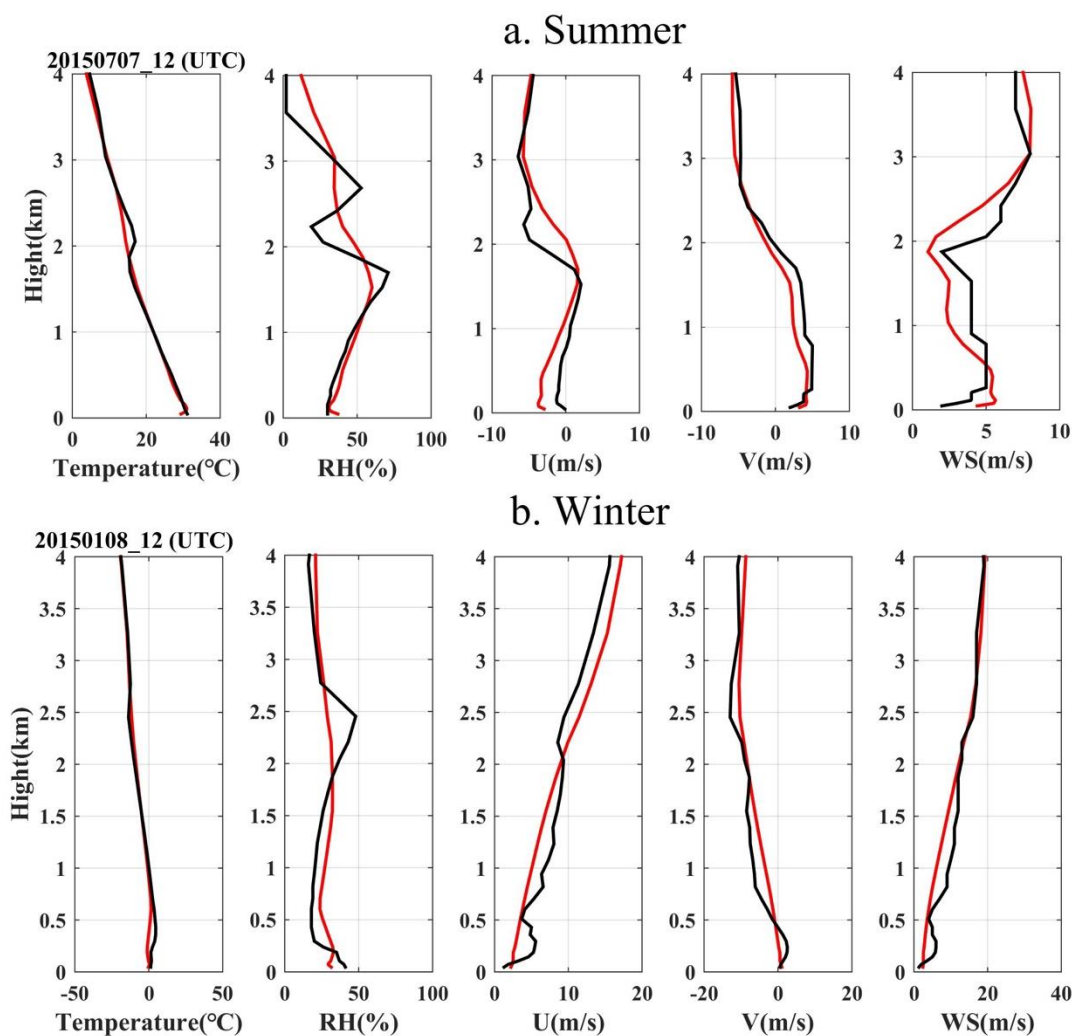
Figure 10. The vertical profile comparisons of temperature (unit: ℃), RH (unit: %), U-wind speed (unit:
360 m/s), V-wind speed (unit: m/s) and wind speed (unit: m/s) at (a) 20150708-12:00 BJT in summer and (b) 20150107-12:00 BJT in winter. The red lines are simulation results, the black lines are observation data.

Figure 11 depicts the averaged diurnal variations of UHII differences (ΔUHII) between UHII with aerosol radiation effect (ARE) and UHII without ARE, with negative values meaning the reduction of UHII by

365   aerosols reduce UHII and positive values showing the opposite. In summer (Figure 11 a), aerosols reduce UHII throughout all day; but in winter (Figure 11 b), aerosols enhance UHII in the afternoon. These results are consistent with the observational results shown in Figure 3. The averaged diurnal variation of downward shortwave radiation at the surface (SWDOWN) between urban and rural areas shows that the SWDOWN difference between urban and rural areas in summer is larger than that in winter (Figure S8).

370   The results in Figure S6 and S8 indicate that the spatial difference of air pollution in summer is larger than that in winter, and the wintertime pollution is more serious than summertime pollution, which is consistent with observational results shown in Figures 5-6. Figure S9 shows the model simulated temperature reductions below 1.5 km, suggesting the ARE is more significant on the temperature lapse rate in winter than that in summer in both urban and rural areas. Moreover, the temperature lapse rate in

375   summer is far more than that in winter. They are also consistent with the observational results shown in Figure 9.
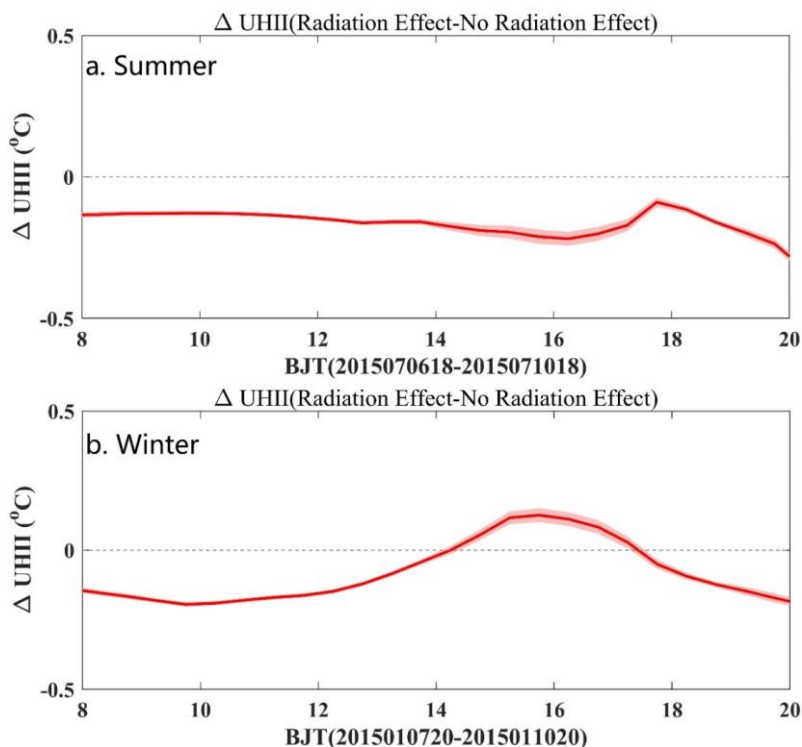
Figure 11. The average diurnal variation of UHII differences ($\Delta UHII$ unit: ℃) between UHII with ARE and UHII without ARE for typical days in (a) summer and (b) winter.

380

5. Conclusion and discussions

Satellite, ground-based, sounding data and WRF-Chem mods were used to analyze the UHII under polluted and clean conditions at 35 cities in China. Seasonal differences in UHII between summer and winter were also compared. On an annual basis, aerosols reduce the UHII, which is consistent with previous work (Wu et al. 2017). In summer, aerosols reduce the UHII, but in winter, aerosols enhance the UHII. Furthermore, we used the concepts of the Spatial Discrepancy in Aerosol Radiative Effect (SD-ARE) and the Dynamic Effect (DE) to explain how aerosols influence the UHII in different seasons. We then verified The mechanisms by means of observational analyses and model simulations.

In summer, airflow changes slightly within the PBL under polluted conditions. There is still a strong heat release and heat exchange between urban and rural areas, so the dynamic effect is weak. The spatial discrepancy in aerosol radiative effect differs between urban and rural areas because of the inhomogeneous spatial distribution of air pollution between these two areas. Since urban pollution is often more severe than rural pollution, less solar radiation reaches urban areas than in rural areas. The urban temperature enhancement is thus weaker under polluted conditions than clean ones, weakening the UHII. Figure 12a shows a diagram of how aerosols influence the UHII in summer.

In winter, the spatial discrepancy in aerosol radiative effect is weak but the dynamic effect is significant under polluted conditions in winter. Concerning the spatial discrepancy in aerosol radiative effect, the spatial difference of air pollution between urban and rural areas is small, and urban and rural areas likely experience the same severe pollution, this heats the atmosphere and reduces the similar amount of solar radiation reaching the urban and rural ground. Concerning the dynamic effect, airflow intensity and temperature gradients significantly decrease, stabilizing the PBL and weakening the heat release and heat exchange. Since pollution conditions in both urban and rural areas are similar, the spatial discrepancy in aerosol radiative effect is not a major factor causing higher UHIIs. the dynamic effect weakens airflow, reducing temperature gradients significantly, which in turn, reduces the heat exchange between urban and

385

390

395

400

405   rural areas and the surface heat release. Increasing heat thus accumulates in urban areas, thereby increasing the UHII. Figure 12b shows a diagram of how aerosols influence the UHII in winter.

Our analysis shows the seasonally different effects of aerosols on the UHII and explains the different mechanisms in different seasons, and the mechanism summary is shown in tables at the bottom of Figures 12a and 12b. Although this study comprehensively explains potential aerosol effects, other effects may

410   be at play such as land surface and aerosol properties (e.g., absorbing versus scattering aerosols). More work needs to be done to verify this. Additionally, this study analyzed observations made at 35 cities located in China and some results of a few cities that were at odds with generalized findings of 35 cities; the different results in some cities may be due to the unique characteristics of these cities regarding their location, terrain, climatic background, etc. This warrants further investigations.
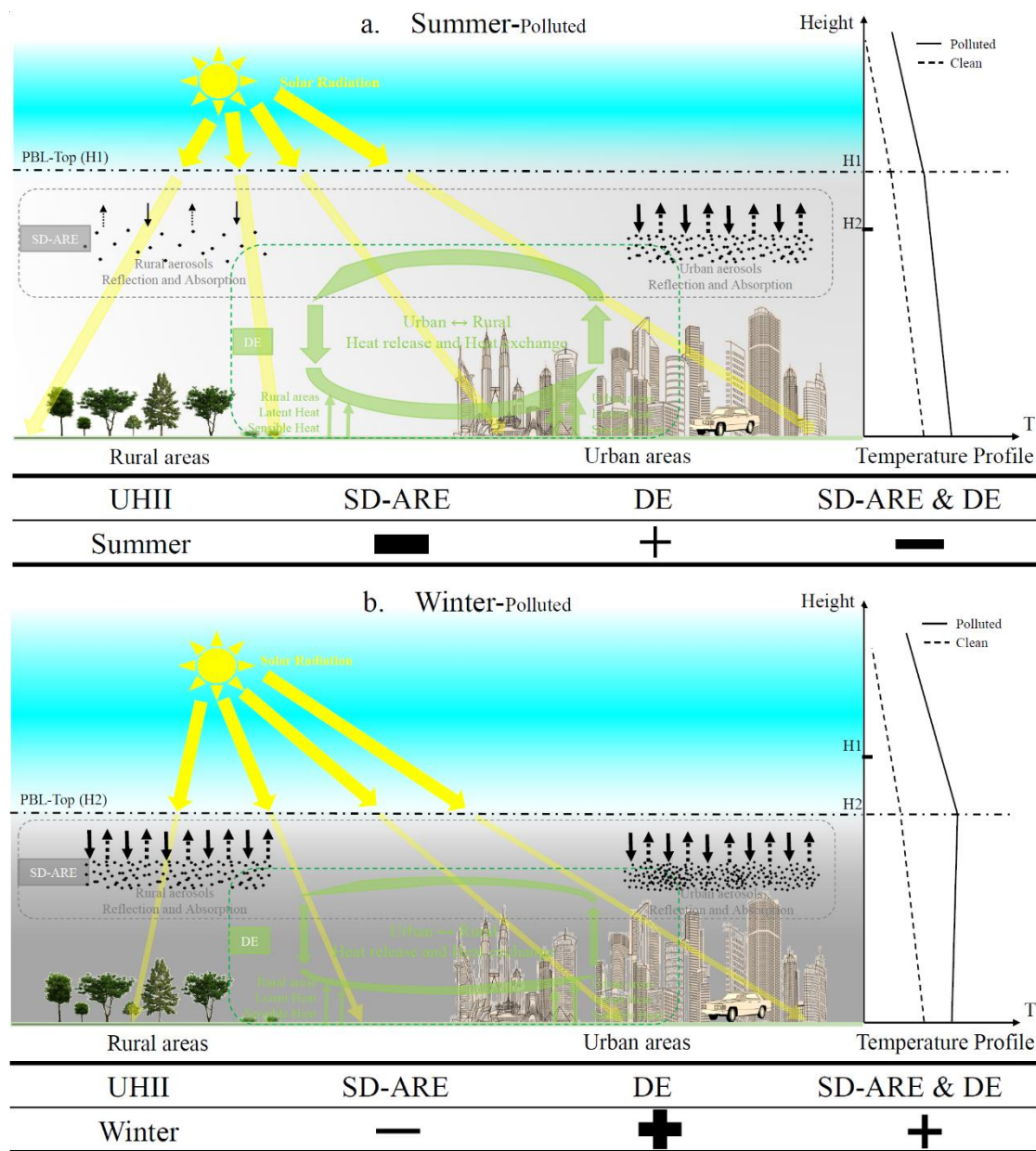
Figure 12 Aerosol effects on the UHII in (a) summer and (b) winter under polluted conditions. The background brightness indicates pollution intensity. Yellow arrows show the solar radiation, and their width indicates the amount of solar radiation to the ground. Green arrows denote heat, and their width indicates heat intensity. Black points and arrows show the process of aerosol-radiation-interaction. Temperature profiles reflect the vertical temperature gradient under clean and polluted conditions. The plus sign means positive effect, while the minus sign means a negative effect.

Atmospheric
Chemistry
and Physics
Discussions

Data availability

The Landsat data, MODIS LST and MAIAC AOD can be download from

425 https://search.earthdata.nasa.gov/. Hourly PM2.5 data is published in real time by the China National

Environmental Monitoring Center (CNEMC, http://www.cnemc.cn/). National Centers for

Environmental Prediction/National Weather Service/NOAA/U.S. Department of Commerce (2000):

NCEP FNL Operational Model Global Tropospheric Analyses, continuing from July 1999. Research Data

Archive at the National Center for Atmospheric Research, Computational and Information Systems

430 Laboratory. Dataset. Accessed 22 Feb. 2019. https://doi.org/10.5065/D6M043C6.

Author contributions

All authors made substantial contributions to this work. HWC and LZQ designed this research. HWC

conducted the analyses and wrote the draft under the supervision of LZQ. LZQ reviewed and edited this

435 paper. WF and ZYW conducted the WRF-Chem simulation and helped to edit this paper. GJP and STN

provided part of datasets and helped to edit this paper. MC reviewed and edited this paper. CTM and WJ

provided part of datasets. LSS gave many suggestions about model simulations.

Competing interests

440 The authors declare that they have no conflict of interest.

Acknowledgements

References

Ackerman, B., Changnon, S., Dzurisin, G., Gatz, D. L., and Grosh, R. C.): Summary of METROMEX, volume 2: causes of precipitation anomalies, 1978.

Bornstein, R., and Lin, Q.: Urban heat islands and summertime convective thunderstorms in Atlanta: three case studies, Atmospheric Environment, 34(3): 507-516, https://doi.org/10.1016/S1352-2310(99)00374-X, 2000.

Cao, C., Lee, X., Liu, S., Schultz, N., Xiao, W., Zhang, M., and Zhao, L.: Urban heat islands in China enhanced by haze pollution, Nature communications , 7(1), 1-7, https://doi.org/10.1038/ncomms12509, 2016.

Carrió, G. and Cotton, W.: Urban growth and aerosol effects on convection over Houston. Part II: Dependence of aerosol effects on instability, Atmospheric research, 102(1): 167-174, https://doi.org/10.1016/j.atmosres.2011.06.022, 2011.

Carrió, G. G., Cotton, W. R., and Cheng, W. Y. Y.: Urban growth and aerosol effects on convection over Houston: Part I: The August 2000 case, Atmospheric Research, 96(4): 560-574, https://doi.org/10.1016/j.atmosres.2010.01.005, 2010.

Changnon, S. A., Huff, F. A., Schickedanz, P. T., and Vogel, J. L.: Summary of METROMEX, Volume 1: Weather anomalies and impacts, 1977.

Changnon, S. A., Shealy, R. T., and Scott, R. W.: Precipitation changes in fall, winter, and spring caused by St. Louis, Journal of Applied Meteorology, 30(1): 126-134, https://doi.org/10.1175/1520-0450(1991)030<0126:PCIFWA>2.0.CO;2, 1991.

Changnon, S. A., and Westcott, N. E.: Heavy rainstorms in Chicago: Increasing frequency, altered impacts, and future implications, JAWRA Journal of the American Water Resources Association, 38(5): 1467-1475, https://doi.org/10.1111/j.1752-1688.2002.tb04359.x, 2002.

Chapman, E. G., Gustafson Jr, W. I., Easter, R. C., Barnard, J. C., Ghan, S. J., Pekour, M. S., and Fast, J. D.: Coupling aerosol-cloud-radiative processes in the WRF-Chem model: Investigating the radiative impact of elevated point sources, Atmospheric Chemistry and Physics, 9(3): 945-964, https://doi.org/10.5194/acp-9-945-2009, 2009.

Chen, F., and Dudhia, J.: Coupling an advanced land surface–hydrology model with the Penn State–NCAR MM5 modeling system. Part I: Model implementation and sensitivity, Monthly Weather

Review, 129(4): 569-585, https://doi.org/10.1175/1520-0493(2001)129<0569:CAALSH>2.0.CO;2, 2001.

Chen, F., Kusaka, H., Bornstein, R., Ching, J., Grimmond, C., Grossman‑Clarke, S., Loridan, T., Manning, K. W., Martilli, A., and Miao, S.: The integrated WRF/urban modelling system: development, evaluation, and applications to urban environmental problems, International Journal of Climatology, 31(2): 273-288, https://doi.org/10.1002/joc.2158, 2011.

Chen, S. H., and Sun, W. Y.: A one-dimensional time dependent cloud model, Journal of the Meteorological Society of Japan. Ser. II, 80(1): 99-118, https://doi.org/10.2151/jmsj.80.99, 2002.

Chýlek, P., and Coakley, J. A.: Aerosols and climate, Science, 183(4120): 75-77, https://doi.org/10.1126/science.183.4120.75, 1974.

Chylek, P., and Wong, J.: Effect of absorbing aerosols on global radiation budget, Geophysical research letters, 22(8): 929-931, https://doi.org/10.1029/95GL00800, 1995.

Cohen, A.J., Brauer, M., Burnett, R., Anderson, H.R., Frostad, J., Estep, K., Balakrishnan, K., Brunekreef, B., Dandona, L., Dandona, R., and Feigin, V.: Estimates and 25-year trends of the global burden of disease attributable to ambient air pollution: an analysis of data from the Global Burden of Diseases Study 2015, The Lancet, 389(10082): 1907-1918, https://doi.org/10.1016/S0140-6736(17)30505-6, 2017.

Ding, A. J., Huang, X., Nie, W., Sun, J. N., Kerminen, V. M., Petäjä, T., et al.: Enhanced haze pollution by black carbon in megacities in China, Geophysical Research Letters, 43(6), 2873-2879, https://doi.org/10.1002/2016GL067745, 2016.

Fallmann, J., Forkel, R., and Emeis, S.: Secondary effects of urban heat island mitigation measures on air quality, Atmospheric Environment, 125: 199-211, https://doi.org/10.1016/j.atmosenv.2015.10.094, 2016.

Fan, J., Leung, L. R., Rosenfeld, D., Chen, Q., Li, Z., Zhang, J., and Yan, H.: Microphysical effects determine macrophysical response for aerosol impacts on deep convective clouds, Proceedings of the National Academy of Sciences, 110(48): E4581-E4590, https://doi.org/10.1073/pnas.1316830110, 2013.

Gedzelman, S. D., Austin, S., Cermak, R., Stefano, N., Partridge, S., Quesenberry, S., and Robinson, D.
505   A.: Mesoscale aspects of the urban heat island around New York City, Theoretical and Applied
       Climatology, 75(1): 29-42, https://doi.org/10.1007/s00704-002-0724-2, 2003.

Givati, A., and Rosenfeld, D.: Quantifying precipitation suppression due to air pollution, Journal of
       Applied   Meteorology,   43(7):   1038-1056,   https://doi.org/10.1175/1520-
       0450(2004)043<1038:QPSDTA>2.0.CO;2, 2004.

510 Grell, G. A., Peckham, S. E., Schmitz, R., McKeen, S. A., Frost, G., Skamarock, W. C., and Eder, B.:
       Fully coupled "online" chemistry within the WRF model, Atmospheric Environment, 39(37): 6957-
       6975, https://doi.org/10.1016/j.atmosenv.2005.04.027, 2005.

Grimmond, S. U. E.: Urbanization and global environmental change: local effects of urban warming, The
       Geographical Journal, 173(1): 83-88, https://doi.org/10.1111/j.1475-4959.2007.232_3.x, 2007.

515 Guenther, A., Karl, T., Harley, P., Wiedinmyer, C., Palmer, P. I., and Geron, C.: Estimates of global
       terrestrial isoprene emissions using MEGAN (Model of Emissions of Gases and Aerosols from
       Nature), Atmospheric Chemistry and Physics, 6.11: 3181-3210, https://doi.org/10.5194/acp-6-3181-
       2006, 2006.

Guo, J., Deng, M., Lee, S. S., Wang, F., Li, Z., Zhai, P., Liu, H., Lv, W., Yao, W., and Li, X.: Delaying
520   precipitation and lightning by air pollution over the Pearl River Delta. Part I: Observational analyses,
       Journal   of   Geophysical   Research: Atmospheres,   121:   6472–6488,
       https://doi.org/10.1002/2015JD023257, 2016a.

Guo, J., Miao, Y., Zhang, Y., Liu, H., Li, Z., Zhang, W., He, J., Lou, M., Yan, Y., Bian, L., and Zhai, P.:
       The climatology of planetary boundary layer height in China derived from radiosonde and reanalysis
525   data, Atmospheric Chemistry and Physics, 16: 13309–13319, https://doi.org/10.5194/acp-16-13309-
       2016, 2016b.

Guo, J., Liu, H., Li, Z., Rosenfeld, D., Jiang, M., Xu, W., Jiang, J. H., He, J., Chen, D., Min, M., and Zhai,
       P.: Aerosol-induced changes in the vertical structure of precipitation: a perspective of TRMM
       precipitation   radar,   Atmospheic   Chemistry   and   Physics,   18:   13329–13343,
530   https://doi.org/10.5194/acp-18-13329-2018, 2018.

Han, J. Y., Baik, J. J., and Khain, A. P.: A numerical study of urban aerosol impacts on clouds and precipitation, Journal of the Atmospheric Sciences, 69(2): 504-520, https://doi.org/10.1175/JAS-D-11-071.1, 2012.

Han, J. Y., Baik, J. J., and Lee, H.: Urban impacts on precipitation, Asia-Pacific Journal of Atmospheric Sciences, 50(1): 17-30, https://doi.org/10.1007/s13143-014-0016-7, 2014.

Heilig, G. K.: World urbanization prospects: the 2011 revision, United Nations, Department of Economic and Social Affairs (DESA), Population Division, Population Estimates and Projections Section, New York, 14, 2012.

Hong, S. Y., Noh, Y., and Dudhia, J.: A new vertical diffusion package with an explicit treatment of entrainment processes, Monthly Weather Review, 134(9): 2318-2341, https://doi.org/10.1175/MWR3199.1, 2006.

Huete, A. R.: A soil-adjusted vegetation index (SAVI), Remote Sensing of Environment, 25(3): 295-309, https://doi.org/10.1016/0034-4257(88)90106-x, 1988.

Iacono, M. J., Delamere, J. S., Mlawer, E. J., Shephard, M. W., Clough, S. A., & Collins, W. D.: Radiative forcing by long‐lived greenhouse gases: Calculations with the AER radiative transfer models, Journal of Geophysical Research: Atmospheres, 113(D13), https://doi.org/10.1029/2008JD009944, 2008.

Jáuregui, E., and Romales, E.: Urban effects on convective precipitation in Mexico City, Atmospheric Environment, 30(20): 3383-3389, https://doi.org/ 10.1016/1352-2310(96)00041-6, 1996.

Kain, J. S.: The Kain–Fritsch convective parameterization: an update, Journal of Applied Meteorology, 43(1): 170-181, https://doi.org/10.1175/1520-0450(2004)043<0170:TKCPAU>2.0.CO;2, 2004.

Kain, J. S., and Fritsch J. M.: A one-dimensional entraining/detraining plume model and its application in convective parameterization, Journal of the Atmospheric Sciences, 47(23): 2784-2802, https://doi.org/10.1175/1520-0469(1990)047<2784:AODEPM>2.0.CO;2, 1990.

Kain, J. S., and Fritsch, J. M.: Convective parameterization for mesoscale models: The Kain-Fritsch scheme, The representation of cumulus convection in numerical models, Springer, 165-170, https://doi.org/10.1007/978-1-935704-13-3_16, 1993.

Kalnay, E., and Cai M.: Impact of urbanization and land-use change on climate, Nature, 423(6939): 528-531, https://doi.org/10.1038/nature01675, 2003.

560 Kaspersen, P. S., Ravn, N. H., Arnbjerg-Nielsen, K., Madsen, H., and Drews, M.: Influence of urban land cover changes and climate change for the exposure of European cities to flooding during high-intensity precipitation, Proceedings of the International Association of Hydrological Sciences (IAHS), 370: 21-27, https://doi.org/10.5194/piahs-370-21-2015, 2015.

Khain, A., Rosenfeld, D., and Pokrovsky, A.: Aerosol impact on the dynamics and microphysics of deep

565 convective clouds, Quarterly Journal of the Royal Meteorological Society, 131(611): 2639-2663, https://doi.org/10.1256/qj.04.62, 2005.

Kim, Y. H., and Baik, J. J.: Maximum urban heat island intensity in Seoul, Journal of Applied Meteorology, 41(6): 651-659, https://doi.org/10.1175/1520-0450(2002)041<0651:MUHIII>2.0.CO;2, 2002.

570 Kug, J. S., and Ahn, M. S.: Impact of urbanization on recent temperature and precipitation trends in the Korean peninsula, Asia-Pacific Journal of Atmospheric Sciences, 49(2): 151-159, https://doi.org/10.1007/s13143-013-0016-z, 2013.

Kusaka, H., and Kimura, F.: Coupling a single-layer urban canopy model with a simple atmospheric model: Impact on urban heat island simulation for an idealized case, Journal of the Meteorological

575 Society of Japan. Ser. II, 82(1): 67-80, https://doi.org/10.2151/jmsj.82.67, 2004.

Kusaka, H., Kondo, H., Kikegawa, Y., and Kimura, F.: A simple single-layer urban canopy model for atmospheric models: Comparison with multi-layer and slab models, Boundary-layer meteorology, 101(3): 329-358, https://doi.org/10.1023/A:1019207923078, 2001.

Lai, L.-W.: The influence of urban heat island phenomenon on PM concentration: an observation study

580 during the summer half-year in metropolitan Taipei, Taiwan, Theoretical and Applied Climatology, 131(1-2), 227-243, https://doi.org/10.1007/s00704-016-1975-7, 2016.

Lee, S. S., and Feingold, G.: Aerosol effects on the cloud-field properties of tropical convective clouds, Atmospheric Chemistry and Physics, 13(14): 6713-6726, https://doi.org/ 10.5194/acp-13-6713-2013, 2013.

585   Li, J., Chen, H., Li, Z., Wang, P., Cribb, M., and Fan, X.: Low-level temperature inversions and their
           effect on aerosol condensation nuclei concentrations under different large-scale synoptic circulations,
           Advances in Atmospheric Sciences, 32(7): 898-908, https://doi.org/10.1007/s00376-014-4150-z,
           2015.

        Li, Z.: Influence of absorbing aerosols on the inference of solar surface radiation budget and cloud
590   absorption,   Journal   of   Climate,   11(1):   5-17,   https://doi.org/10.1175/1520-
           0442(1998)011<0005:IOAAOT>2.0.CO;2, 1998.

        Li, Z., Guo, J., Ding, A., Liao, H., Liu, J., Sun, Y., Wang, T., Xue, H., Zhang H., and Zhu B.: Aerosol
           and boundary-layer interactions and impact on air quality, National Science Review, 4(6): 810-833,
           https://doi.org/ 10.1093/nsr/nwx117, 2017.

595   Li, Z., Lau, W. M., Ramanathan, V., Wu, G., Ding, Y., Manoj, M. G., Liu, J., Qian, Y., Li J., and Zhou
           T. et al.: Aerosol and monsoon climate interactions over Asia, Reviews of Geophysics, 54(4): 866-
           929, https://doi.org/10.1002/2015RG000500, 2016.

        Li, Z., Niu, F., Fan, J., Liu, Y., Rosenfeld, D., and Ding, Y.: Long-term impacts of aerosols on the vertical
           development   of   clouds   and   precipitation,   Nature   Geoscience,   4(12):   888-894,
600   https://doi.org/10.1038/ngeo1313, 2011.

        Li, Z., Rosenfeld, D., and Fan, J.: Aerosols and their Impact on Radiation, Clouds, Precipitation & Severe
           Weather Events, In Oxford Research Encyclopedia of Environmental Science, https://doi.org/
           10.1093/acrefore/9780199389414.013.126, 2017.

        Liao, J., Wang, T., Jiang, Z., Zhuang, B., Xie, M., Yin, C., Wang, X., Zhu, J., Fu Y., and Zhang, Y.:
605   WRF/Chem modeling of the impacts of urban expansion on regional climate and air pollutants in
           Yangtze   River   Delta,   China,   Atmospheric   Environment,   106:   204-214,
           https://doi.org/10.1016/j.atmosenv.2015.01.059, 2015.

        Lin, Y. L., Farley, R. D., and Orville, H. D.: Bulk parameterization of the snow field in a cloud model,
           Journal of Climate and Applied Meteorology, 22(6): 1065-1092, https://doi.org/10.1175/1520-
610   0450(1983)022<1065:BPOTSF>2.0.CO;2, 1983.

Liu, H., Guo, J., Koren, I., Altaratz, O., Dagan, G., Wang, Y., Jiang, J. H., Zhai, P., and Yung, Y.: Non-monotonic aerosol effect on precipitation in convective clouds over tropical oceans, Scientific Reports, 9, 7809, https://doi.org/10.1038/s41598-019-44284-2, 2019.

Liu, S., Liu, Z., Li, J., Wang, Y., Ma, Y., Sheng, L., Liu, H., Liang, F., Xin, G., and Wang J.: Numerical simulation for the coupling effect of local atmospheric circulations over the area of Beijing, Tianjin and Hebei Province, Science in China Series D: Earth Sciences, 52(3): 382-392, https://doi.org/10.1007/s11430-009-0030-2, 2009.

Liu, T., Gong, S., He, J., Yu, M., Wang, Q., Li, H., Liu, W., Zhang, J., Li, L., and Wang X.: Attributions of meteorological and emission factors to the 2015 winter severe haze pollution episodes in China's Jing-Jin-Ji area, Atmospheric Chemistry and Physics, 17(4): 2971-2980, https://doi.org/10.5194/acp-17-2971-2017, 2017.

Lou, M., Guo, J., Wang, L., Xu, H., Chen, D., Miao, Y., Lv, Y., Li, Y., Guo, X., Ma, S., and Li, J.: On the relationship between aerosol and boundary layer height in summer in China under different thermodynamic conditions, Earth and Space Science, 6(5): 887-901, https://doi.org/10.1029/2019EA000620, 2019.

Lyapustin, A., Martonchik, J., Wang, Y., Laszlo, I., and Korkin, S.: Multiangle implementation of atmospheric correction (MAIAC): 1. Radiative transfer basis and look‐up tables, Journal of Geophysical Research: Atmospheres, 116(D3), https://doi.org/10.1029/2010JD014985, 2011a.

Lyapustin, A., Wang, Y., Laszlo, I., Kahn, R., Korkin, S., Remer, L., Levy, R., and Reid, J.: Multiangle implementation of atmospheric correction (MAIAC): 2. Aerosol algorithm, Journal of Geophysical Research: Atmospheres, 116(D3), https://doi.org/10.1029/2010JD014986, 2011b.

Lyapustin, A. I., Wang, Y., Laszlo, I., Hilker, T., Hall, F. G., Sellers, P. J., Tucker, C. J., and Korkin, S. V.: Multi-angle implementation of atmospheric correction for MODIS (MAIAC): 3. Atmospheric correction, Remote Sensing of Environment, 127: 385-393, https://doi.org/10.1016/j.rse.2012.09.002, 2012.

Miao, S., Chen, F., LeMone, M. A., Tewari, M., Li, Q., and Wang, Y.: An observational and modeling study of characteristics of urban heat island and boundary layer structures in Beijing, Journal of

Applied Meteorology and Climatology, 48(3): 484-501, https://doi.org/10.1175/2008JAMC1909.1, 2009.

640 Monin, A. S., and Obukhov, A. M.: Basic laws of turbulent mixing in the surface layer of the atmosphere, Contrib. Geophys. Inst. Acad. Sci. USSR, 151(163): e187.

Morris, C. J. G., and Simmonds, I.: Associations between varying magnitudes of the urban heat island and the synoptic climatology in Melbourne, Australia, International Journal of Climatology, 20(15): 1931-1954, https://doi.org/10.1002/1097-0088(200012)20:15<1931::AID-JOC578>3.0.CO;2-D, 645 2000.

Morrison, H., Thompson, G., and Tatarskii, V.: Impact of cloud microphysics on the development of trailing stratiform precipitation in a simulated squall line: Comparison of one-and two-moment schemes, Monthly weather review, 137(3): 991-1007, https://doi.org/10.1175/2008MWR2556.1, 2009.

650 Oke, T. R.: The energetic basis of the urban heat island, Quarterly Journal of the Royal Meteorological Society, 108(455): 1-24, https://doi.org/10.1002/qj.49710845502, 1982.

Petäjä, T., Järvi, L., Kerminen, V. M., Ding, A. J., Sun, J. N., Nie, W., Kujansuu, J., Virkkula, A., Yang, X., and Fu, C.: Enhanced air pollution via aerosol-boundary layer feedback in China, Scientific reports, 6, 18998, https://doi.org/10.1038/srep18998, 2016.

655 Pinto Jr, O., Pinto, I. R. C. A., and Ferro, M. A. S. A study of the long‐term variability of thunderstorm days in southeast Brazil, Journal of Geophysical Research: Atmospheres, 118(11): 5231-5246, https://doi.org/10.1002/jgrd.50282, 2013.

Qi, J., Chehbouni, A., Huete, A. R., Kerr, Y. H., and Sorooshian, S.: A modified soil adjusted vegetation index, Remote sensing of environment, 48(2): 119-126, https://doi.org/10.1016/0034-660 4257(94)90134-1, 1994.

Rondeaux, G., Steven, M., and Baret, F.: Optimization of soil-adjusted vegetation indices, Remote sensing of environment, 55(2): 95-107, https://doi.org/10.1016/0034-4257(95)00186-7, 1996.

Rosenfeld, D., Lohmann, U., Raga, G. B., O'Dowd, C. D., Kulmala, M., Fuzzi, S., Reissell, A., and Andreae M. O.: Flood or drought: how do aerosols affect precipitation?, Science, 321(5894): 1309-665 1313, https://doi.org/10.1126/science.1160606, 2008.

Ryu, Y. H., and Baik, J. J.: Quantitative analysis of factors contributing to urban heat island intensity, Journal of Applied Meteorology and Climatology, 51(5): 842-854, https://doi.org/10.1175/JAMC-D-11-098.1, 2012.

Sakulyanontvittaya, T., Duhl, T., Wiedinmyer, C., Helmig, D., Matsunaga, S., Potosnak, M., Milford J. and Guenther, A.: Monoterpene and sesquiterpene emission estimates for the United States, Environmental Science & Technology, 42(5), 1623-1629, https://doi.org/10.1021/es702274e, 2008.

Sanap, S. D., and Pandithurai, G.: Inter‑annual variability of aerosols and its relationship with regional climate over Indian subcontinent, International Journal of Climatology, 35(6): 1041-1053, https://doi.org/10.1002/joc.4037, 2015.

Shepherd, J. M., and Burian, S. J.: Detection of urban-induced rainfall anomalies in a major coastal city, Earth Interactions, 7(4): 1-17, https://doi.org/10.1175/1087-3562(2003)007<0001:DOUIRA>2.0.CO;2, 2003.

Shepherd, J. M., Pierce, H., and Negri, A. J.: Rainfall modification by major urban areas: Observations from spaceborne rain radar on the TRMM satellite, Journal of Applied Meteorology, 41(7): 689-701, https://doi.org/10.1175/1520-0450(2002)041<0689:RMBMUA>2.0.CO;2, 2002.

Snyder, W. C., Wan, Z., Zhang, Y., and Feng, Y. Z.: Classification-based emissivity for land surface temperature measurement from space, International Journal of Remote Sensing, 19(14): 2753-2774, https://doi.org/10.1080/014311698214497, 1998.

Taha, H.: Urban climates and heat islands: albedo, evapotranspiration, and anthropogenic heat, Energy and buildings, 25(2): 99-103, https://doi.org/10.1016/S0378-7788(96)00999-1, 1997.

Tao, W. K., Simpson, J., and McCumber, M.: An ice-water saturation adjustment, Monthly Weather Review, 117(1): 231-235, https://doi.org/10.1175/1520-0493(1989)117<0231:AIWSA>2.0.CO;2, 1989.

Tao, W., Liu, J., Ban-Weiss, G. A., Hauglustaine, D. A., Zhang, L., Zhang, Q., Cheng, Y., Yu, Y. and Tao, S.: Effects of urban land expansion on the regional meteorology and air quality of eastern China, Atmos. Chem. Phys, 15(15): 8597-8614, https://doi.org/10.5194/acp-15-8597-2015, 2015.

Wan, Z., and Dozier, J.: A generalized split-window algorithm for retrieving land-surface temperature from space, IEEE Transactions on geoscience and remote sensing, 34(4): 892-905, https://doi.org/10.1109/36.508406, 1996.

Wang, K., Dickinson, R. E., and Liang, S.: Clear sky visibility has decreased over land globally from 1973 to 2007, Science, 323(5920): 1468-1470, https://doi.org/10.1126/science.1167549, 2009.

Wang, K., and Liang, S.: Evaluation of ASTER and MODIS land surface temperature and emissivity products using long-term surface longwave radiation observations at SURFRAD sites, Remote Sensing of Environment, 113(7): 1556-1565, https://doi.org/10.1016/j.rse.2009.03.009, 2009.

Wang, Y., Wan, Q., Meng, W., Liao, F., Tan, H., and Zhang, R.: Long-term impacts of aerosols on precipitation and lightning over the Pearl River Delta megacity area in China, Atmospheric Chemistry and Physics, 11(23): 12421-12436, https://doi.org/10.5194/acp-11-12421-2011, 2011.

Wei, J., Huang, W., Li, Z., Xue, W., Peng, Y., Sun, L. and Cribb, M.: Estimating 1-km-resolution $PM_{2.5}$ concentrations across China using the space-time random forest approach, Remote Sensing of Environment, 231, 111221, https://doi.org/10.1016/j.rse.2019.111221, 2019a.

Wei, J., Li, Z., Guo, J., Sun, L., Huang, W., Xue, W., Fan, T, and Cribb, M.: Satellite-derived 1-km-resolution PM_1 concentrations from 2014 to 2018 across China, Environ. Sci. Tech., 53(22), 13,265–13,274, https://doi.org/10.1021/acs.est.9b03258, 2019b.

Wei, J., Li, Z., Peng, Y., Sun, L., and Yan, X.: A regionally robust high-spatial-resolution aerosol retrieval algorithm for MODIS images over Eastern China, IEEE T. Geosci. Remote, 57(7), 4748–4757, 2019c.

Wiedinmyer, C., Akagi, S. K., Yokelson, R. J., Emmons, L. K., Al-Saadi, J. A., Orlando, J. J., and Soja, A. J.: The Fire INventory from NCAR (FINN): A high resolution global model to estimate the emissions from open burning, Geoscientific Model Development, 4(3), 625, https://doi.org/10.5194/gmd-4-625-2011, 2011.

Wu, H., Wang, T., Riemer, N., Chen, P., Li, M., and Li, S.: Urban heat island impacted by fine particles in Nanjing, China, Scientific reports, 7(1): 11422, https://doi.org/10.1038/s41598-017-11705-z, 2017.

Atmospheric
Chemistry
and Physics
Discussions

720   Wu, J., Fu, C., Zhang, L., and Tang, J.: Trends of visibility on sunny days in China in the recent 50 years, Atmospheric Environment, 55: 339-346, https://doi.org/10.1016/j.atmosenv.2012.03.037, 2012.

Yang, B., Yang, X., Leung, L. R., Zhong, S., Qian, Y., Zhao, C., Chen, F., Zhang, Y., and Qi, J.: Modeling the Impacts of Urbanization on Summer Thermal Comfort: The Role of Urban Land Use and Anthropogenic Heat, Journal of Geophysical Research: Atmospheres, 124, no. 13:6681-6697,
725   PNNL-SA-147485, https://doi.org/10.1029/2018JD029829, 2019

Yang, X., Ruby Leung, L., Zhao, N., Zhao, C., Qian, Y., Hu, K., and Liu, X. et al.: Contribution of urbanization to the increase of extreme heat events in an urban agglomeration in East China, Geophysical Research Letters, 44, no. 13:6940-6950. PNNL-SA-127213. https://doi.org/10.1002/2017GL074084, 2017.

730   Yang, X., Ferrat, M., and Li, Z.: New evidence of orographic precipitation suppression by aerosols in central China, Meteorology and Atmospheric Physics, 119(1-2): 17-29, https://doi.org/10.1007/s00703-012-0221-9, 2013.

Yang, Y., Gao, Z., Shi, T., Wang, H., Li, Y., Zhang, N., Zhang, H., and Huang, Y.: Assessment of urban surface thermal environment using MODIS with a population-weighted method: a case study.
735   Journal of Spatial Science, 64(2), 287-300, https://doi.org/10.1080/14498596.2017.1422155, 2019.

Yang, Y., Zheng, Z., Yim, S. Y., Roth, M., Ren, G., Gao, Z., Wang, T., Li, Q., Shi, C., Ning, G., and Li, Y.: PM2. 5 Pollution Modulates Wintertime Urban Heat Island Intensity in the Beijing-Tianjin-Hebei Megalopolis, China. Geophysical Research Letters, 47(1), e2019GL084288, https://doi.org/10.1029/2019GL084288, 2020.

740   Yu, W., Ma, M., Wang, X., Song, Y., and Tan, J.: Validation of MODIS land surface temperature products using ground measurements in the Heihe River Basin, China, Remote Sensing for Agriculture, Ecosystems, and Hydrology XIII (Vol. 8174, p. 817423), International Society for Optics and Photonics, https://doi.org/10.1117/12.897571, 2011.

Zaveri, R. A., Easter, R. C., Fast, J. D., and Peters, L. K.: Model for simulating aerosol interactions and
745   chemistry (MOSAIC), Journal of Geophysical Research: Atmospheres, 113(D13), https://doi.org/10.1029/2007JD008782, 2008.

Atmospheric
Chemistry
and Physics
Discussions
Open Access
EGU

Zaveri, R. A., and Peters, L. K.: A new lumped structure photochemical mechanism for large‑scale applications, Journal of Geophysical Research: Atmospheres, 104(D23): 30387-30415, https://doi.org/10.1029/1999JD900876, 1999.

750   Renhe, Z., Li, Q., and Zhang, R.: Meteorological conditions for the persistent severe fog and haze event over eastern China in January 2013, Science China Earth Sciences, 57(1): 26-35, https://doi.org/10.1007/s11430-013-4774-3, 2014.

Zhang, W., Guo, J., Miao, Y., Liu, H., Song, Y., Fang, Z., He, J., Lou, M., Yan, Y., Li, Y., and Zhai, P.: On the summertime planetary boundary layer with different thermodynamic stability in China: A
755   radiosonde perspective, Journal of Climate, 31(4): 1451-1465, https://doi.org/10.1175/JCLI-D-17-0231.1, 2018.

Zhang, Z., Wu, W., Fan, M., Wei, J., Tan, Y., and Wang, Q.: Evaluation of MAIAC aerosol retrievals over China, Atmospheric Environment , 202, 8-16, https://doi.org/10.1016/j.atmosenv.2019.01.013, 2019.

760   Zhao, L., Lee, X., Smith, R. B., and Oleson, K.: Strong contributions of local background climate to urban heat islands, Nature, 511(7508): 216-219, https://doi.org/10.1038/nature13462, 2014.

Zhao, M., Cai, H., Qiao, Z., and Xu, X.: Influence of urban expansion on the urban heat island effect in Shanghai, International Journal of Geographical Information Science, 30(12): 2421-2441, https://doi.org/10.1080/13658816.2016.1178389, 2016.

765   Zhong, S., Qian, Y., Sarangi, C., Zhao, C., Leung, R., Wang, H., and Yang, B.: Urbanization effect on winter haze in the Yangtze River Delta region of China, Geophysical Research Letters, 45, 6710–6718, https://doi.org/10.1029/2018GL077239, 2018

Zhong, S., Qian, Y., Zhao, C., Leung, R., Wang, H., Yang, B., and Liu, D: Urbanization-induced urban heat island and aerosol effects on climate extremes in the Yangtze River Delta region of China,
770   Atmospheric Chemistry and Physics, 17(8), 5439–5457, https://doi.org/ 10.5194/acp-17-5439-2017, 2017.

Zhou, D., Zhang, L., Hao, L., Sun, G., Liu, Y., and Zhu, C.: Spatiotemporal trends of urban heat island effect along the urban development intensity gradient in China, Science of the Total Environment, 544: 617-626, https://doi.org/10.1016/j.scitotenv.2015.11.168, 2016.

775 Zhou, D., Zhao, S., Zhang, L., Sun, G., and Liu, Y.: The footprint of urban heat island effect in China, Scientific reports, 5(1), 1-11, https://doi.org/10.1038/srep11160 , 2015.

Zhang, Z., Wu, W., Fan, M., Wei, J., Tan, Y., and Wang, Q.: Evaluation of MAIAC aerosol retrievals over China. Atmospheric Environment, 202, 8-16, 2019.